Optimizing Imbalance and Loss in 2 × 2 3-dB Multimode Interference Couplers via Access Waveguide Width

Martin T. Hill, *Associate Member, IEEE*, X. J. M. Leijtens, G. D. Khoe, *Fellow, IEEE*, and M. K. Smit, *Senior Member, IEEE*

***Abstract*—The imbalance and excess loss in multimode interference couplers with fabrication errors are examined. Remarkably, there exists a number of optimum access waveguide widths which give a minimum imbalance. Furthermore, quite low excess loss can be simultaneously achieved by choosing one particular optimum width. It is also shown that paired interference couplers have better imbalance performance than general interference couplers, given the same fabrication tolerances and length constraint for both coupler types. In particular, a paired interference coupler with an access waveguide width approximately 0.3 times the coupler width has the best imbalance performance. These results are obtained using a simple model and are supported by more sophisticated numerical models and experimental data from couplers fabricated in InP/InGaAsP.**

***Index Terms*—Integrated optics, multimode interference (MMI) couplers, multimode waveguides, optical couplers, optical waveguide components, optical waveguides, photonic integrated circuits.**

I. Introduction

In RECENT years, multimode interference (MMI) couplers [1] have become one of the most important types of directional coupler used in integrated optics. MMI couplers have many advantages, such as small size, wavelength and polarization insensitivity, and insensitivity to fabrication errors [2].

Probably the most widely used MMI coupler is the 2 × 2 3-dB coupler, where power in each of the two inputs is split equally between the two outputs. These couplers are often used in various types of integrated optical interferometers.

Two of the most important characteristics of a 3-dB coupler are the excess loss and the imbalance between the two outputs. Excess loss and imbalance are typically caused by deviations from the design dimensions, which occur due to fabrication tolerances. Imbalance is particularly important when the couplers are used in Mach–Zehnder interferometers (MZIs)for optical switches [3]. A power imbalance in the two arms of the MZI results in a reduction of the output contrast ratio.

A generic MMI coupler, along with its access waveguides, is shown in Fig. 1. Power to input port 1 P_1 is split equally between the output ports 3 and 4 P_3, P_4. The total coupler length L_T consists of the MMI section length L and the taper lengths 2 $L_{\rm tap}$. The tapers are required to adapt the waveguide width used in the rest of the system W_g to the MMI section access waveguide width W_a. It is desirable to make L_T as small as possible, given the imbalance and excess loss requirements and the fabrication tolerances.

This paper investigates the effects of the access waveguide width and position on the imbalance and excess loss of the coupler. It is shown that for all 2 × 2 3-dB MMI couplers, there exists a number of optimum access waveguide widths that give a minimum imbalance. Furthermore, these widths are different to the W_a that gives a minimum excess loss. This knowledge of the optimum widths for imbalance and excess loss can be employed by the designer to obtain a coupler with the minimum L_T, given requirements and fabrication tolerances. In addition, the performance of general and paired interference couplers are compared [1] when they are subjected to the same constraints and tolerances.

Previous work on fabrication tolerances and their effect on excess loss have used a Gaussian beam model of the light propagating in and out of the access waveguides [2]. However, this model offers little insight into the causes of imbalance. In this paper, a simple model based on sinusoidal modes is employed [4]. It is shown that the general results obtained with the simple model match well those obtained with more sophisticated numerical models [5]. The results of the simple model are further confirmed with experimental results from couplers made in InP/InGaAsP.

The rest of the paper is organized as follows. In Section II, a simple model for the coupler is developed and the causes of imbalance and loss discussed. Section III presents and discusses numerical results from the model. The fabricated couplers are described and results from measurements are given in Section IV. Finally, Section V concludes the paper.

II. MMI Coupler Model

In integrated optics, structures are often formed on a semiconductor wafer on which there are several layers of different compositions. Typically, there are three layers, consisting of a high-refractive-index light-guiding layer, sandwiched between two lower refractive index layers. Waveguides are commonly formed by etching away the material surrounding the waveguide, forming a ridge waveguide. Fig. 2 shows such a waveguide where the guiding layer is InGaAsP. Typically, there is

Manuscript received October 28, 2002; revised June 30, 2003. This research was supported by the Netherlands Organization for Scientific Research (N.W.O.) through the "NRC Photonics" grant.

The authors are with the COBRA Research Institute, Department of Electrical Engineering, EH 12.33, Eindhoven University of Technology, 5600 MB Eindhoven, The Netherlands.

Digital Object Identifier 10.1109/JLT.2003.818164

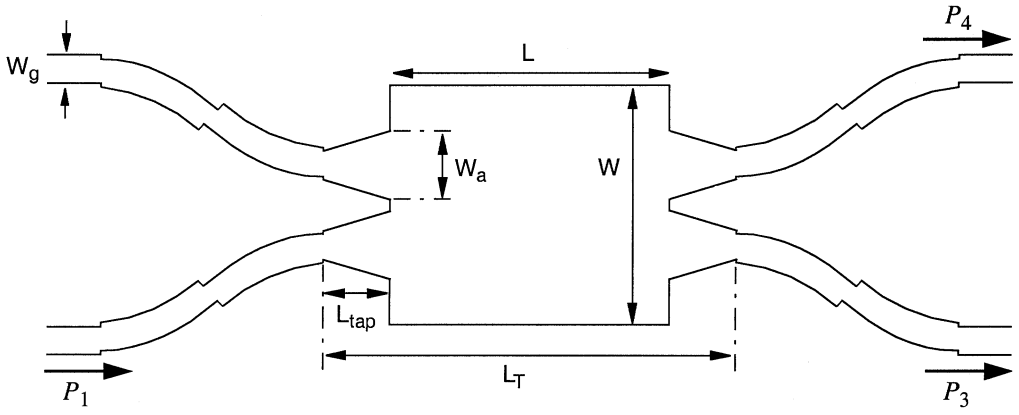

Fig. 1. General structure of MMI coupler with access waveguides.

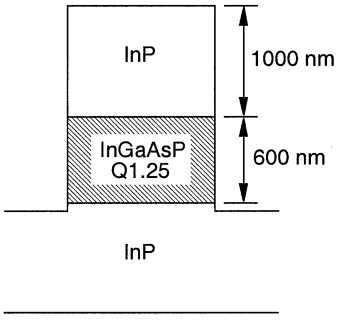

Fig. 2. Cross section of ridge waveguide employed to make MMI couplers.

a step-index change between the waveguide ridge and the surrounding material.

Fig. 3 show a two-dimensional (2-D) representation of the MMI coupler and access waveguides. It is assumed that the lateral (x axis) dimensions of the waveguides are much larger than the transverse dimensions (y axis). The transverse dimension is just 600 nm in the couplers reported here (Fig. 2). In the transverse direction, the waveguide structure is assumed to be single mode and have the same characteristics everywhere. These assumptions allow the three-dimensional (3-D) physical waveguide to be replaced by a 2-D waveguide using techniques such as the effective-index method [6]. The effective index of the waveguide ridge is denoted n_r. The effective index of the cladding around the waveguides is denoted n_c.

The lateral index contrast can be maximized by deep etching through the light-guiding layer [7]. Furthermore, deep etching eliminates uncertainties in index contrast and effective waveguide widths due to etch-depth tolerances. These uncertainties can be significant in shallow-etched waveguides, where only part of the guiding layer is etched.

The MMI section guides m lateral modes numbered $\nu = 0, 1, 2, \ldots m-1$. MMI modes with even ν are called even modes, and MMI modes with odd ν are called odd modes. Only one lateral waveguide mode in the access waveguides of width W_a is considered, mode 0. The access waveguide may guide higher order modes; however, the curved system waveguides of width W_g will typically strongly attenuate higher order modes. Furthermore, it is assumed that only mode 0 will be intentionally excited in the input access waveguide.

With high lateral index contrast, the lateral penetration of the mode field outside the waveguide is negligible. Thus, the mode-field profiles $\psi_\nu(x)$ can be approximated by sinusoids. For the MMI section

$$\psi_\nu(x) = \sin\left[\pi(\nu+1)\frac{x}{W}\right]. \tag{1}$$

The access waveguide mode 0 is also approximated by a sinusoid. The field profile at the input of the MMI section ($z = 0$) is as follows when only input port one is excited:

$$\Psi(x,0) = \begin{cases} \sin\left[\frac{\pi\left(x - x_c + \frac{W_a}{2}\right)}{W_a}\right], & x_c - \frac{W_a}{2} < x < x_c + \frac{W_a}{2} \\ 0, & \text{otherwise} \end{cases}. \tag{2}$$

The input light distribution can be expressed as the weighted sum of the modes of the MMI section, with ν extending to infinity, as follows:

$$\Psi(x,0) = \sum_{\nu=0}^{\infty} c_\nu \psi_\nu(x). \tag{3}$$

The approach employed in [4] is used to obtain the mode weights c_ν. The weights for the modes are the Fourier series coefficients of a periodic odd function. This function is constructed with $\Psi(x,0)$ for $0 \le x < W$, and $-\Psi(-x,0)$ for $-W < x < 0$. The $2W$ long interval from $-W$ to W is repeated in the $\pm x$ directions to form the periodic function. The Fourier series coefficients c_ν for the periodic odd function are

$$\begin{aligned} c_\nu &= \frac{2}{W}\int_{x_c-\frac{W_a}{2}}^{x_c+\frac{W_a}{2}} \sin\left[\frac{\pi\left(x - x_c + \frac{W_a}{2}\right)}{W_a}\right]\sin\left[\pi(\nu+1)\frac{x}{W}\right]dx \\ &= \frac{4W_a}{\pi W\left(1-(\nu+1)^2\left(\frac{W_a}{W}\right)^2\right)}\cos\left[\pi(\nu+1)\frac{W_a}{2W}\right] \\ &\quad \times \sin\left[\pi(\nu+1)\frac{x_c}{W}\right]. \end{aligned} \tag{4}$$

Note that the reconstruction of the input light field with the MMI modes is only approximate when the number of modes is limited to m.

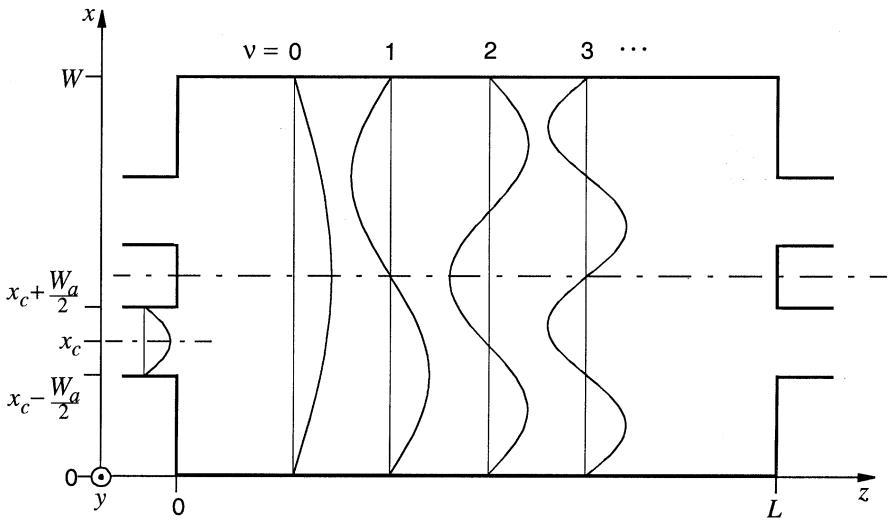

Fig. 3. MMI section and access waveguides showing the access waveguide mode 0 and the first four modes of the MMI section. The placement of the access waveguides is symmetric about the center line. Also shown is the coordinate system.

The modes propagate with different propagation constants β_ν in the longitudinal (z) direction. The length L_π, the beat length of the two lowest order modes, is found in [1] to be

$$L_\pi = \frac{\pi}{\beta_0 - \beta_1} \approx \frac{4n_r W^2}{3\lambda_0}. \tag{5}$$

The difference between the propagation constants for the ν^{th} mode and the lowest order mode is found in [1] using the paraxial approximation to be

$$\beta_0 - \beta_\nu = \frac{\nu(\nu+2)\pi}{3L_\pi}. \tag{6}$$

The phase rotation of the mode ν electric field with respect to mode 0, as the modes travel a distance of z along the MMI section, is simply $(\beta_0 - \beta_\nu)z$. Thus, the phase of the mode ν field with respect to mode 0 at the end of the MMI section is

$$\phi_\nu = \frac{\nu(\nu+2)\pi L}{3L_\pi}. \tag{7}$$

It has been shown in [1] that, due to this phase rotation, single or multiple images of the input field may be formed at special positions along the z axis. By choosing the MMI section length L to correspond to one of the these special positions and by placing the output waveguides appropriately, various types of couplers or splitters can be formed [1].

This paper concentrates on 2 × 2 3-dB couplers. Here, two images of an input are formed. For an arbitrary input waveguide position x_c, the L required to form two images is 1.5 L_π [1]. This type of coupler is referred to as a general interference coupler. Having the input waveguides centered on the positions $x = W/3$ and $2W/3$ causes $c_\nu = 0$ for $\nu = 2, 5, 8, \ldots$. The L required to form two images is only 0.5 L_π with this special positioning of the waveguides. This type of coupler is referred to as a paired interference coupler [1]. The images at L appear at the same x-axis positions as the input waveguides.

Note that two images of the input waveguides will also be formed at multiples of the lengths mentioned previously. However, generally, the shortest coupler is of most interest, and therefore, couplers using multiples of the lengths given previously are not considered.

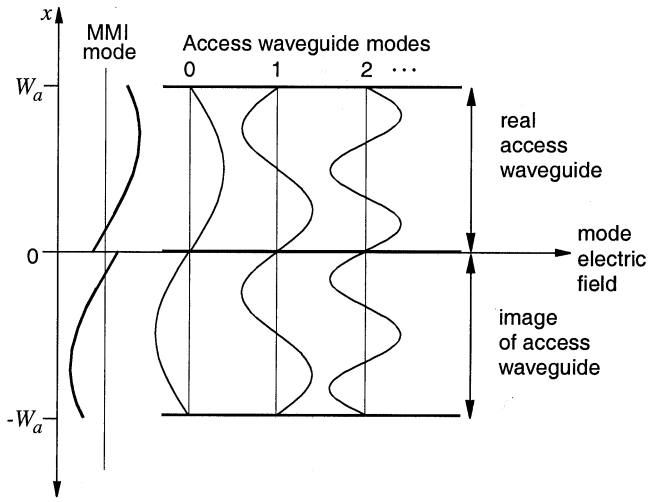

Fig. 4. Section of MMI mode-field profile at output access waveguide and the access waveguide modes. Fourier techniques are used to obtain the contribution of the MMI mode to mode 0 in the output waveguide. The MMI mode-field profile and access waveguide modes are inverted and mirrored about the line $x = 0$. The interval from $-W_a$ to W_a is repeated in the $\pm x$ directions to form a periodic odd function, the first Fourier coefficient of which gives the contribution to mode 0.

At the end of the MMI waveguide, optical power is either transferred into the output waveguides or lost out the end of the MMI waveguide. Reflections from the MMI waveguide ends are not considered, as they have been shown to be small, even in high-contrast waveguides [8]. Each MMI waveguide mode contributes to the mode 0 field in the output waveguide. The final strength of the mode 0 field in an output waveguide will be the vector sum of all the MMI mode contributions.

How much an MMI mode ν contributes to the mode 0 field can be found using Fourier techniques. Fig. 4 shows the output waveguide, a section of a MMI mode-field profile at the entrance of the output waveguide, and some of the output waveguide modes. Note that the zero point on the x axis has been shifted by $x_c - W_a/2$ for convenience. The MMI mode electric field outside the access waveguide will have no effect on the

field in the access waveguide and is ignored. The MMI mode ν field profile at the access waveguide input can be represented by a Fourier series using the access waveguide modes as the set of basis functions. To obtain the Fourier series that will represent the MMI mode field with a set of sine functions, the MMI mode-field profile must be presented as a periodic odd function. The periodic odd function is made by first reflecting an inverted copy of the MMI mode field about the line $x = 0$ (see Fig. 4). Then, the interval from $-W_a$ to $+W_a$ is repeated in the $\pm x$ directions. The same reflection and repetition is performed for the access waveguide and its modes.

Only the lowest Fourier coefficient is required, and this is found for the MMI mode ν as $b_{0\nu}$, as follows:

$$b_{0\nu} = \frac{2}{W_a}\int_0^{W_a} \sin\left[\frac{\pi(\nu+1)\left(x + x_c - \frac{W_a}{2}\right)}{W}\right]\sin\left[\frac{\pi x}{W_a}\right]dx = \frac{W}{W_a}c_\nu. \tag{8}$$

Note that it has been assumed that the input and output waveguides have the same widths W_a.

For the even MMI modes, $b_{0\nu}$ is the same for both output waveguides. However, for odd MMI modes, the sign of $b_{0\nu}$ is opposite for each output waveguide. This sign change is due to the odd symmetry of the odd MMI modes, about the MMI section center line [1].

When the MMI section length L is precisely $1.5\,L_\pi$, or $0.5\,L_\pi$ for the paired interference coupler, then for even MMI modes, $\phi_\nu = 0$ (7). For odd modes, $\phi_\nu = -\pi/2$ for general interference couplers, and $\phi_\nu = \pi/2$ for paired interference couplers.

Each MMI mode contribution to the output waveguide mode 0 has amplitude $b_{0\nu}$ and phase ϕ_ν. The vector representing the amplitude and phase for mode 0 in the output waveguide is the result of adding two vectors: one vector is the vector sum of all the even MMI mode contributions, the even vector; the other vector is the sum of all the odd MMI mode contributions, the odd vector. These vectors for the two output waveguides are shown in Fig. 5 for paired interference.

The fabrication tolerance that is most significant for MMI couplers is the variation of the MMI section width [2]. The deviation ΔW from the design width W causes the design length to deviate by ΔL from the length at which the desired images are obtained. ΔW can be related to ΔL via (5), as follows:

$$\frac{|\Delta L|}{L} = \frac{2|\Delta W|}{W}. \tag{9}$$

The ΔL causes the phases ϕ_ν to diverge from the ideal 0 or $\pi/2$ by $\Delta\phi_\nu$. The phase error $\Delta\phi_\nu$ for mode ν can be found using (7) as follows:

$$\Delta\phi_\nu = \frac{\nu(\nu+2)\pi}{3}\frac{L}{L\pi}\frac{\Delta L}{L}. \tag{10}$$

The phase errors cause the odd and even vectors to be rotated from their ideal positions by $\Delta\phi_o$ and $\Delta\phi_e$, respectively (Fig. 5), as follows:

$$\Delta\phi_o = \arg\left[\sum_{\nu\ \text{odd}} c_\nu^2 \exp(j\Delta\phi_\nu)\right] \tag{11}$$

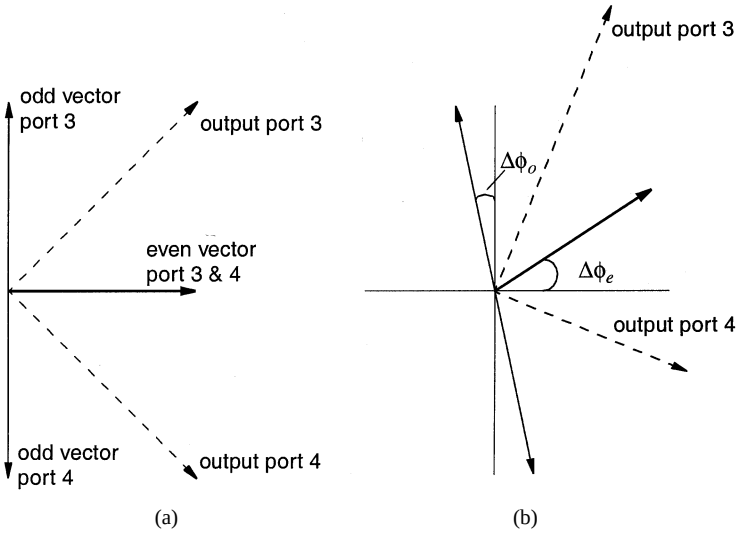

Fig. 5. Construction of the output amplitudes and phases from the even and odd MMI mode contributions: (a) when there are no phase errors and (b) when there are phase errors, due to an error in the MMI section length. The difference between the phase errors in the odd vector $\Delta\phi_o$ and the even vector $\Delta\phi_e$ leads to imbalance in the outputs.

$$\Delta\phi_e = \arg\left[\sum_{\nu\ \text{even}} c_\nu^2 \exp(j\Delta\phi_\nu)\right]. \tag{12}$$

The magnitude of the odd and even vectors can also be found

$$M_o = \frac{W}{W_a}\left|\sum_{\nu\ \text{odd}} c_\nu^2 \exp(j\Delta\phi_\nu)\right| \tag{13}$$

$$M_e = \frac{W}{W_a}\left|\sum_{\nu\ \text{even}} c_\nu^2 \exp(j\Delta\phi_\nu)\right|. \tag{14}$$

If the $\Delta\phi_\nu$ and c_ν are such that $\Delta\phi_o = \Delta\phi_e$, then the odd and even vectors contribute equally to each output, giving no imbalance. However, if $\Delta\phi_o \neq \Delta\phi_e$, then the magnitude of the sum of the odd and even vectors will be different for the two outputs, producing imbalance. The imbalance can be defined as

$$\text{Imbalance} = 10\log\frac{P_3}{P_4}. \tag{15}$$

The imbalance can be expressed in terms of the vector magnitudes and phase errors for small $\Delta\phi_e - \Delta\phi_o$.

$$\text{Imbalance} \sim 10\log\left(1 + \frac{4M_oM_e\sin(\Delta\phi_e - \Delta\phi_o)}{M_o^2 + M_e^2}\right). \tag{16}$$

From (16), it can be seen that the imbalance is primarily determined by $|\Delta\phi_e - \Delta\phi_o|$. This phase difference is determined by c_ν. $|\Delta\phi_e - \Delta\phi_o|$ can be kept small if the effect of $\Delta\phi_\nu$ of an even mode on $\Delta\phi_e$ is the same as the effect of the following odd mode on $\Delta\phi_o$. For large ν, the phase difference between successive modes $\Delta\phi_{\nu+1} - \Delta\phi_\nu$ becomes large (10). Thus, effects of $\Delta\phi_\nu$ on $\Delta\phi_o$ and $\Delta\phi_e$ will not be the same at high ν. To avoid this error, the c_ν must decrease rapidly enough with increasing ν so that the contributions to $\Delta\phi_o$ and $\Delta\phi_e$ at high ν are small. Thus, for small W_a, where the c_ν decrease very slowly, a large imbalance can be expected. However, the relationship

between the c_ν and $|\Delta\phi_e - \Delta\phi_o|$ is complex. Hence, the imbalance does not decrease monotonically with increasing W_a. It will be shown in the next section that there exists a number of local minima and maxima in the imbalance as a function of W_a.

The excess loss of the coupler is defined as

$$\text{Excess Loss} = -10\log\frac{P_3+P_4}{P_1}. \tag{17}$$

The excess loss can be expressed in terms of the vector magnitudes

$$\text{Excess Loss} = -10\log\left[2\left(M_o^2+M_e^2\right)\right]. \tag{18}$$

The vector magnitudes can be decreased in two ways. First, due to the finite number of guided modes m, not all of the input power gets transported to outputs. Second and more important, the contributions from the MMI modes to the odd and even vectors do not constructively add together. This decrease follows directly from (10), as some power is always lost due to the nonzero $\Delta\phi_\nu$. As ν increases, $\Delta\phi_\nu$ increases; hence, the contributions from the higher order modes will contribute less to the vector magnitudes. Power should be concentrated in the lower order modes to decrease the amount of power lost, i.e., the c_ν must decrease rapidly with increasing ν, which can be achieved by increasing W_a. It will be shown in the following section that the excess loss decreases with increasing W_a. This result is in agreement with the findings of [2].

The access waveguide also experiences the width error ΔW, causing the c_ν to be changed slightly. For very small W_a, these effects may be significant. However, for the larger W_a, which are of most interest, the effects will be smaller and therefore are neglected here.

ΔW can also cause the access waveguides to deviate from the $W/3$ and $2W/3$ positions for the paired interference coupler. Simulations indicate that the effects of this error are small in comparison to the effect of ΔL. Hence, this error is not taken into account.

III. Numerical Results and Simulations

To see precisely the dependence of imbalance and excess loss on the access waveguide width and position, (16) and (18) must be evaluated numerically. Fortunately, the Fourier series coefficients c_ν (4) depend only on the normalized access waveguide width and position, that is, W_a/W and x_c/W. Thus, the results obtained are applicable to couplers of any size.

However, there are some aspects that depend somewhat on the specifics of the coupler implementation. First, the tolerances of the manufacturing process will determine ΔW, which eventually determines $\Delta L/L$ and $\Delta\phi_\nu$. Second, the number of guided modes in the MMI section m will be determined by the waveguide material, index contrast, and MMI section width. Finally, the predictions of (16) will differ from reality due to the approximations used to find the propagation constants (6).

All these implementation specific effects become small when the power is concentrated in the lower order MMI modes, that is, small c_ν for high ν. It will be shown that it is this operating region that is most interesting. Furthermore, a realistic ΔW is chosen, and results are given for different numbers of guided modes m. Thus, at the very least, the results presented here provide a good indication of the optimum coupler design, independent of the implementation specifics.

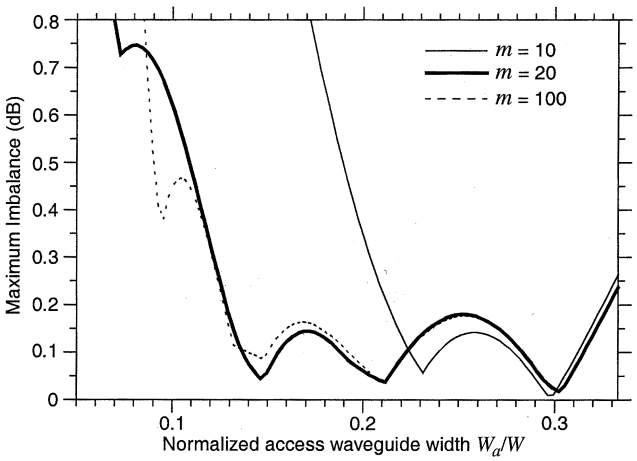

Fig. 6. Maximum imbalance versus normalized access waveguide width for paired interference couplers. Curves are given for various numbers of guided modes m, 10, 20, and 100. The normalized length tolerance $\Delta L/L$ was ± 0.04.

The manufacturing process used to fabricate the couplers described in the next section had a width tolerance ΔW of better than $\pm$ 0.4 μm. The maximum length of the MMI coupler was taken to be 500 μm. With the parameters $n_r = 3.286$, $n_c = 1$, $L = L_\pi/2$ (paired interference), and $\lambda_0 = 1.55$ μm, the MMI section width W was approximately 18.8 μm (5). From these values of ΔW and W, it was decided to choose a maximum $\Delta L/L$ value of ± 0.04 for the paired interference couplers. The waveguide of width 18.8 μm could support 20 modes. Thus, only the first 20 terms in the Fourier series (4) were taken into account, that is, m was chosen to be 20. Results are also presented for $m = 10$ and $m = 100$, where the first 10 and 100 terms, respectively, of the Fourier series were used.

The results in this section give the maximum absolute value of imbalance and excess loss, obtained as $\Delta L/L$ ranges between its two extremes. Fig. 6 shows the maximum imbalance for a paired interference coupler, with $\Delta L/L$ ranging between $+0.04$ and -0.04. The imbalance is shown versus the normalized access waveguide width. It can be seen that, for small access waveguide widths, the imbalance is large. For the case of $m = 20$, as the width increases, the imbalance decreases until a local minimum is reached near 0.15. The imbalance then rises again and falls again. A global minimum is reached near 0.3. For $m = 100$, the imbalance is similar to the 20 mode case. The imbalance when $m = 10$ is considerably higher at small width, than for $m = 20$. Furthermore, the first minimum is shifted to the right. However, note that the global minimum stays at around 0.3 for all three plots of imbalance. Finally, for somewhat higher values of $\Delta L/L$, it can be shown that the global minimum stays near 0.3 and becomes more sharply defined.

Fig. 7 shows the maximum excess loss for the coupler described previously. It can be seen that the excess loss decreases monotonically with increasing access waveguide width. Obtaining the lowest loss requires choosing the largest possible access waveguide width. Excess loss for $m = 10$ is less than for $m = 20$ and $m = 100$ at small W_a/W. The smaller excess

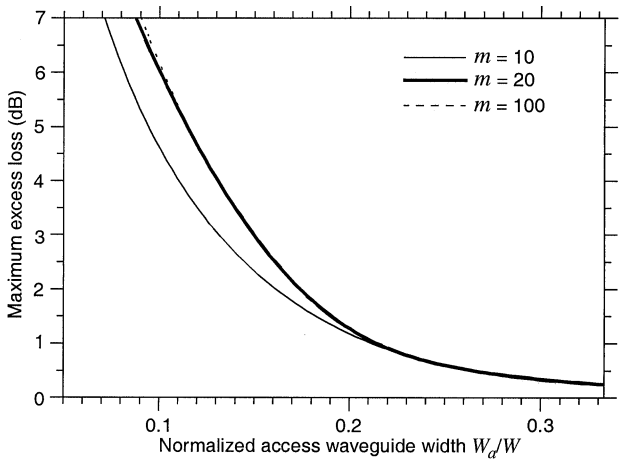

Fig. 7. Maximum excess loss versus normalized access waveguide width for paired interference couplers. Curves are given for various numbers of guided modes m, 10, 20 and 100. The normalized length tolerance $\Delta L/L$ was ± 0.04.

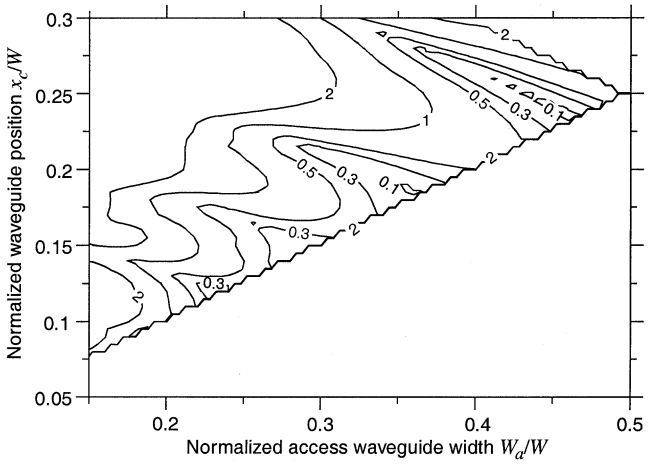

Fig. 8. Contour plot of maximum imbalance versus normalized access waveguide width and normalized access waveguide position for general interference couplers. The number of guided modes was 20. The normalized length tolerance $\Delta L/L$ was $\pm 0.04\sqrt{3}$. Note the imbalance values shown are in decibels.

loss is due to the higher order MMI modes for $m = 20$ and $m = 100$, adding destructively to the lower order modes at the coupler outputs.

The general interference coupler requires $L = 3L_\pi/2$. Thus, W is $\sqrt{3}$ times smaller than for a paired interference coupler (5), given the same constraint on the MMI coupler length. Hence, the relative errors $\Delta W/W$ and $\Delta L/L$ are increased by a factor $\sqrt{3}$, compared with the paired interference coupler. The phase errors (10) are further increased by a factor 3, compared with the paired interference coupler, due to the increased ratio L/L_π.

The general interference coupler allows the free choice of both x_c and W_a. In the plot of maximum imbalance for the general interference coupler (Fig. 8), the horizontal axis is the normalized width W_a/W. The vertical axis is the normalized position of the access waveguide. A contour plot is used to represent the maximum imbalance information in two dimensions. The number of guided MMI modes is kept as 20 to facilitate comparison with the paired interference coupler. Furthermore, the maximum $\Delta L/L$ was $\pm 0.04 \times \sqrt{3}$.

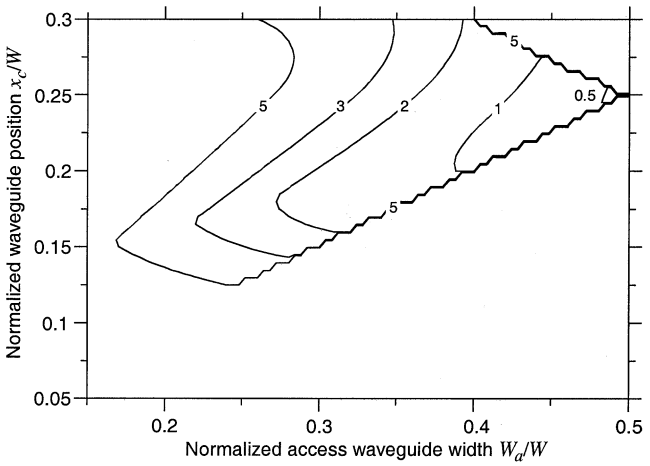

Fig. 9. Contour plot of maximum excess loss versus normalized access waveguide width and normalized access waveguide position for general interference couplers. The number of guided modes was 20. The normalized length tolerance $\Delta L/L$ was $\pm 0.04\sqrt{3}$. Note the loss values shown are in decibels.

Note that due to the decreased width of the general interference coupler, a smaller number of modes are guided than in the paired interference coupler. For example, the general interference coupler only guided 11 modes, when using the same technology and length constraint as for the paired interference coupler mentioned previously. However, the reduced number of modes does not affect the results significantly for large W_a/W, which is the region of most interest.

It can be seen that the maximum imbalance is typically much higher than for the paired interference coupler. This higher imbalance is to be expected due to the total increase in phase errors by the factor $3\sqrt{3}$ mentioned previously. However, remarkably, there are some small regions where very low imbalance can be obtained. Making the MMI sit precisely in these small regions may be difficult. Slight deviations from these regions will incur considerably increased imbalance. The excess loss for the general interference coupler is given in a similar contour plot (Fig. 9).

Having the access waveguides on the outside of the MMI section ($x_c = W_a/2$) appears from Fig. 8 to be the most promising general interference design. Fig. 10 shows the imbalance and excess loss for various W_a/W for a general interference coupler with $x_c = W_a/2$. Comparing Fig. 10 to Fig. 6, it can be clearly seen that the general interference coupler has inferior performance compared with the paired interference coupler.

From Fig. 10, the global imbalance minimum occurs at 0.47 W, after which the imbalance rises sharply, similar to the paired interference coupler trend in Fig. 6. Remarkably, it can be shown using the approach outlined in this paper that 2×2 MMI couplers with splitting ratios 28:72 and 15:85 [9] also have similar imbalance trends and minima.

The specific paired interference coupler design described previously was also simulated using a numerical computer aided design (CAD) tool for integrated optical circuits [5]. This simulation included all the implementation specific effects, in particular, the deviation of the MMI mode profiles from the assumed sinusoidal form, and the deviation of the relative mode

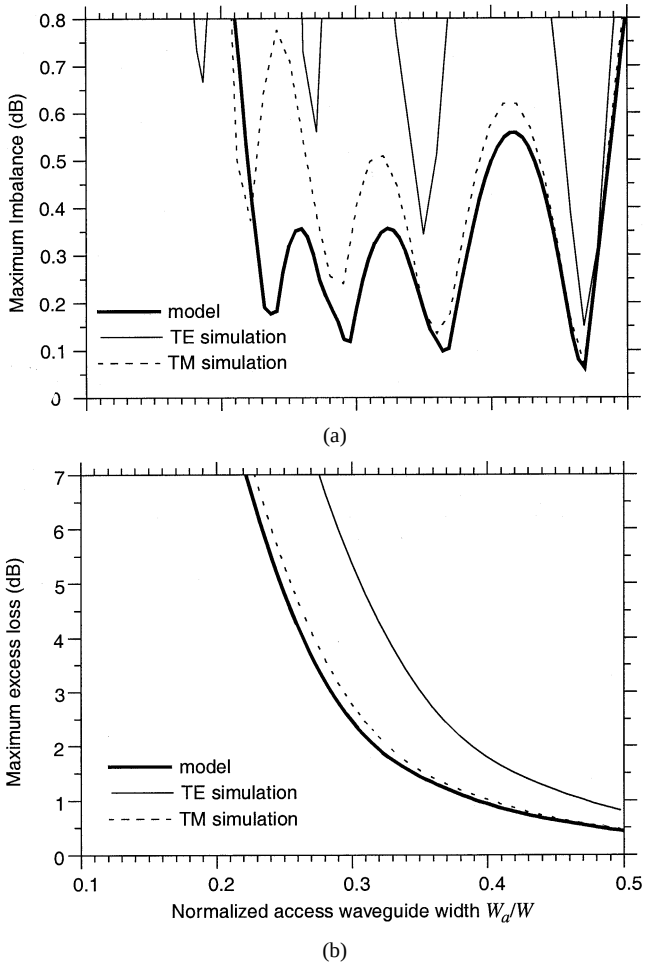

Fig. 10. Plot of maximum imbalance (a) and excess loss (b) versus normalized access waveguide width for a general interference coupler, with the access waveguides at the edge of the MMI section ($x_c = W_a/2$). Results from the model are given for a MMI section that guided 20 modes, and the normalized length tolerance $\Delta L/L$ was $\pm 0.04\sqrt{3}$. Results from a computer-aided design (CAD) simulation tool for optical integrated circuits are also given. Simulation results are presented for both transverse electric (TE)- and transverse magnetic (TM)-polarized light. Note that the simulated results follow the model trends well, even though less MMI modes were present in the simulation.

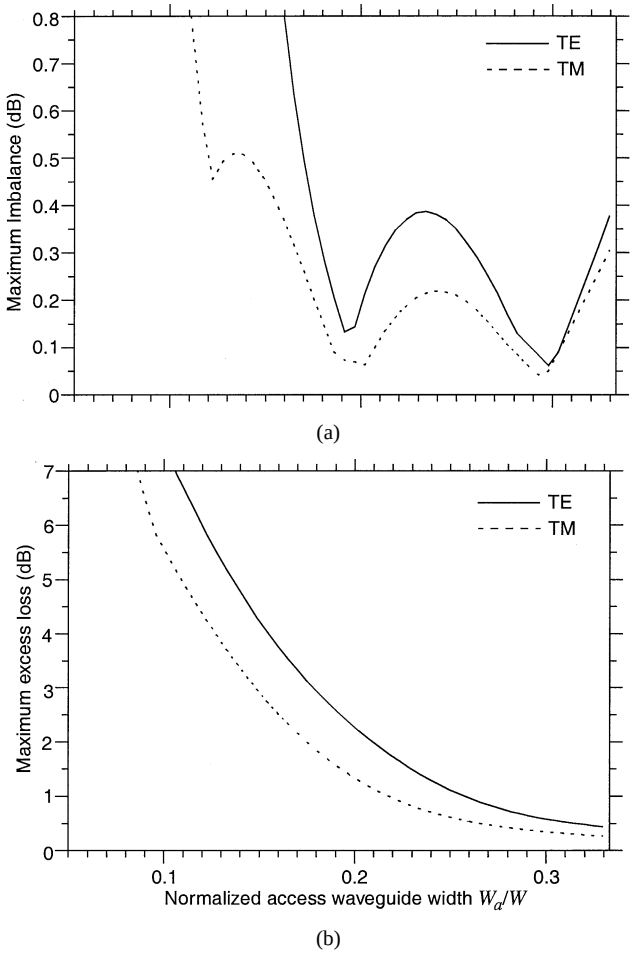

Fig. 11. Predicted maximum imbalance (a) and loss (b) versus normalized access waveguide width for a specific paired interference coupler, made with high index contrast waveguides. Results for both TE- and TM-polarized light are shown. The results were obtained using a CAD simulation tool for optical integrated circuits. It can be seen that imbalance and loss given by the simple generalized model, Fig. 6, predicts well the imbalance and loss given by the simulation tool at large widths. Note that m was 20, and the maximum $\Delta L/L$ was ± 0.04.

phases from (7). The simulation was performed for both transverse electric (TE)- and transverse magnetic (TM)-polarized light. The results of the simulation are given in Fig. 11. It can be seen that the imbalance, although slightly higher, follows the trend predicted by the simple model, particularly at larger widths. The loss also agrees well with that predicted by the simple model.

CAD simulations were also performed for a general interference coupler of length 500 μm. The MMI section width W was approximately 10.9 μm and guided only 11 modes. The simulation results are shown in Fig. 10, and they follow the trends predicted by the simple model. These simulation results for both coupler types indicate that the generalized results from the simple model provide a useful prediction of the MMI coupler performance.

The CAD tool also simulated a paired interference coupler, made with silica on silicon low index contrast waveguides. The waveguide core index n_r was 1.455, and the cladding index n_c was 1.445. The coupler dimensions were chosen so that the MMI section guided 20 modes. The coupler MMI section effective width was 108 μm, and its design length was 7408 μm. A maximum $\Delta L/L$ of ± 0.04 is somewhat unrealistic, given the larger MMI section dimensions. However, to facilitate comparison with the high index contrast coupler described previously, the maximum $\Delta L/L$ was kept the same at ± 0.04.

The simulation results are shown in Fig. 12. The imbalance and loss for this coupler also follow the trends predicted by the simple model, particularly for larger W_a/W. Thus, the predicted optimum W_a/W for an imbalance of around 0.28 to 0.3 is valid for a wide range of specific coupler designs.

IV. Experiment

A number of MMI couplers were fabricated to find the coupler design with minimum imbalance, given a constraint on L_T and, furthermore, to provide experimental data to support the simulation results obtained in the previous section.

The couplers were fabricated using InP/InGaAsP material on a wafer with the following layer structure: an InP substrate, a 600-nm InGaAsP bandgap 1.25-μm guiding layer, and a

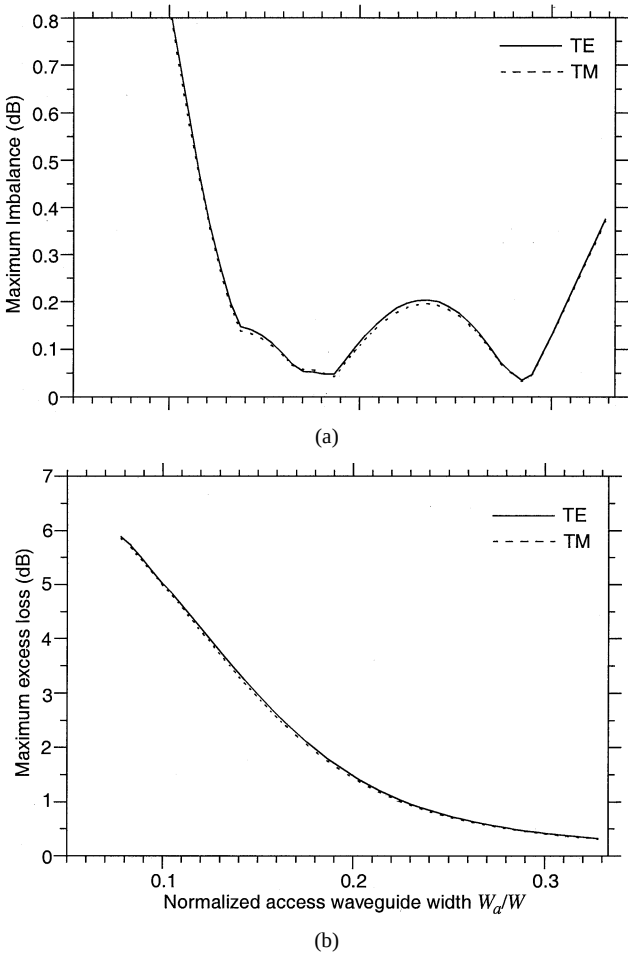

Fig. 12. Further results from the CAD simulation tool, now for a coupler fabricated with silica-on-silicon low index contrast waveguides. Again, the maximum imbalance (a) and loss (b) curves follow the trends predicted by the simple model. To facilitate comparison with the high index contrast coupler, the number of guided modes m was 20, and the maximum $\Delta L/L$ was ± 0.04. Results for both TE- and TM-polarized light are shown.

1000-nm InP top layer (Fig. 2). A 100-nm SiN_x layer served as an etching mask. Lithography transferred the device pattern to the SiN_x layer, which was then etched using CHF_3 reactive ion etching. Further reactive ion etching was used to etch through the top and guiding layers. The effective refractive index of the waveguide ridge was $n_r = 3.286$. Etching through the guiding layer produced an effective index at the sides of the ridge of 1, thus maximizing the lateral index contrast.

The design constraints were as follows: the total coupler length L_T was 500 μm, the standard waveguide width W_g was 2 μm, and $\lambda_0 = 1.55$ μm. Paired interference MMI couplers were made with access waveguide widths W_a of 2, 3, 4, and 5 μm. Adiabatic linear tapers [6] were used to match W_a to W_g. The MMI section lengths L and widths W, and the taper lengths $L_{\rm tap}$ are given in Table I. Note that the actual MMI section widths used were 0.15 μm smaller than that given in the table to take into account the waveguide effective width [1].

The couplers were made in the style shown in Fig. 1. The waveguide separation after the waveguide bends was 20 μm. The four couplers tested were located within 100 μm of each other on the same wafer. Hence, all four couplers should experience the same fabrication errors. Three sets of four couplers were fabricated. Each set was individually processed on a separate wafer quarter.

TABLE I
LIST OF PARAMETERS FOR THE TEST MMI COUPLERS

W_a	L_{tap}	L	W	W_a/W
2 μm	0 μm	500 μm	18.81 μm	0.106
3 μm	14 μm	472 μm	18.28 μm	0.164
4 μm	37 μm	426 μm	17.36 μm	0.230
5 μm	71 μm	358 μm	15.92 μm	0.314

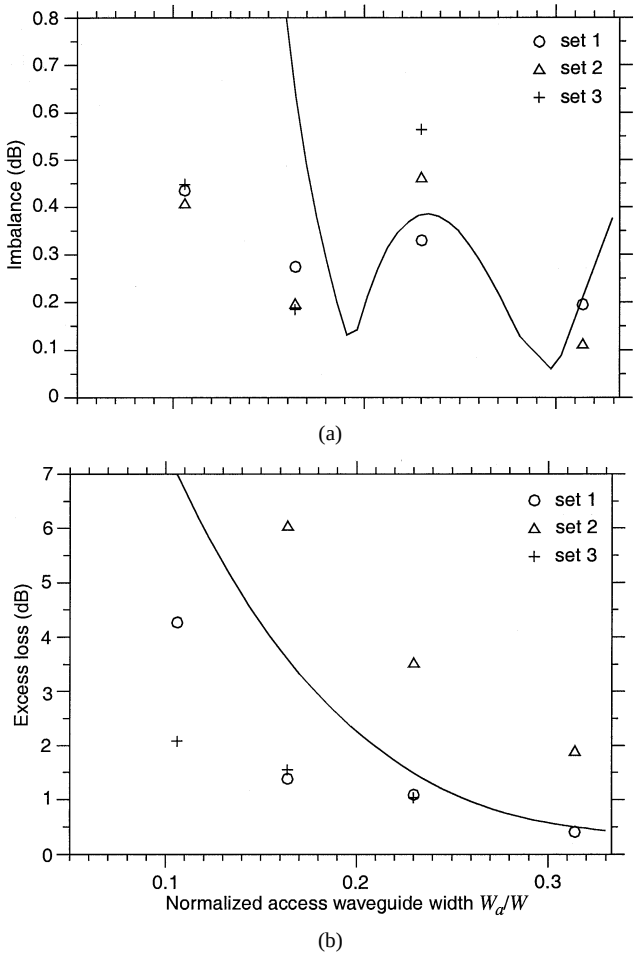

Fig. 13. Measured imbalance and loss versus normalized access waveguide width for the fabricated paired interference couplers. The excess loss decrease monotonically with increased waveguide width. However, the imbalance exhibits multiple maxima and minima. Also shown are the predicted maximum imbalance and loss curves from Fig. 11.

The transmission of light through each coupler was measured as follows: a microscope objective-coupled TE-polarized light produced by an erbium-doped fiber amplifier (EDFA) into one port of the coupler. A lensed fiber tip collected the light at one of the coupler outputs. The output power at wavelength 1.55 μm was measured using an optical spectrum analyzer. The output power was measured relative to the power transmitted through straight reference waveguides. The results are plotted in Fig. 13. The imbalance follows qualitatively the predicted pattern of Figs. 6 and 11(a). Note that the minimum imbalance

occurs close to the optimum normalized width of 0.3. The loss follows the monotonically decreasing trend that was predicted in Figs. 7 and 11(b).

The higher loss in the second set was due to a fault in the waveguides on the input side of the couplers. Furthermore, one of the couplers in the third set did not function, and therefore is not reported in the figures.

It can be seen from both the numerical and experimental results that choosing a W_a/W near 0.3 delivers a coupler with low imbalance and quite a low loss. However, it should be kept in mind that longer tapers decrease the MMI section length, increasing $\Delta W/W$ and $\Delta L/L$. The taper lengths required depend on the specific material and waveguide structure W_g and W_a.

The deeply etched access waveguides strongly confine the light in the waveguide. However, low contrast waveguides, made by only partially etching through the light-guiding layer, are popular due to their low losses. For these low contrast waveguides, the lateral penetration of the mode fields outside the waveguide can be of the order of 1 μm. When employing these waveguides, it is important to account for this increased effective width [1] of W_a when calculating W_a/W.

For large W_a/W, the space between the access waveguides at the taper ends could become filled in due to the finite resolution of the lithographic process. For the paired interference coupler with $W_a = 0.3\,W$, the space between the waveguides is just $0.033\,W$. However, lateral penetration of the mode-field profile outside the waveguide increases the effective width of the waveguide. The larger effective width increases the physical spacing of the waveguides and relaxes the lithographic requirements.

V. Conclusion

The imbalance and excess loss in MMI couplers is primarily determined by the way the input power is partitioned into the MMI section modes. This partitioning is in turn determined by the normalized access waveguide width and position. It was shown that there exists a number of optimum access waveguide widths that give a minimum imbalance. In particular, paired interference couplers were found to have better imbalance performance than general interference couplers, given the same fabrication tolerances. Furthermore, for paired interference couplers, choosing the normalized access waveguide width near 0.3 delivers minimum imbalance, with low excess loss.

A simple model was employed to arrive at the previously mentioned conclusions. The results of the simple model were supported by more sophisticated numerical models and experimental data from fabricated MMI couplers.

The model gives insight into the causes of imbalance in MMI couplers. Furthermore, the results presented here provide guidance to the designer trying to fabricate couplers with minimum imbalance, given a constraint on coupler length. It was shown that couplers with low imbalance and reasonable excess loss can be made by choosing the access waveguide width carefully.

Acknowledgment

The authors would like to thank T. de Vries for his advice in processing the MMI couplers reported in this article. They would also like to thank JDS Uniphase, The Netherlands, for providing the antireflection coating for the couplers reported here.

References

[1] L. B. Soldano and E. C. M. Pennings, "Optical multi-mode interference devices based on self-imaging: principles and applications," *J. Lightwave Technol.*, vol. 13, pp. 615–627, Apr. 1995.

[2] P. A. Besse, M. Bachmann, H. Melchior, L. B. Soldano, and M. K. Smit, "Optical bandwidth and fabrication tolerances of multimode interference couplers," *J. Lightwave Technol.*, vol. 12, pp. 1004–1009, June 1994.

[3] D. H. P. Maat, Y. C. Zhu, F. H. Groen, H. van Brug, H. J. Frankena, and X. J. M. Leijtens, "Polarization independent dilated InP-based space switch with low crosstalk," *IEEE Photon. Technol. Lett.*, vol. 12, pp. 284–286, Mar. 2000.

[4] M. Bachmann, P. A. Besse, and H. Melchior, "General self-imaging properties in N × N multimode interference couplers," *Appl. Opt.*, vol. 33, no. 18, pp. 3905–3911, June 1994.

[5] X. J. M. Leijtens, P. Le Lourec, and M. K. Smit, "S-matrix oriented CAD-tool for simulating complex integrated optical circuits," *IEEE J. Select. Topics Quantum Electron.*, vol. 2, pp. 257–262, June 1996.

[6] T. Tamir, Ed., *Guided-Wave Optoelectronics*. Berlin: Springer-Verlag, 1988, ch. 2, pp. 69–74.

[7] L. H. Spiekman, Y. S. Oei, E. G. Metaal, F. H. Groen, I. Moerman, and M. K. Smit, "Extremely small multimode interference couplers and ultrashort bends on InP by deep etching," *IEEE Photon. Technol. Lett.*, vol. 6, pp. 1008–1010, Aug. 1994.

[8] D. Erasme, L. H. Spiekman, C. G. P. Herben, M. K. Smit, and F. H. Groen, "Experimental assessment of the reflection of passive multimode interference couplers," *IEEE Photon. Technol. Lett.*, vol. 9, pp. 1604–1606, Dec. 1997.

[9] M. Bachmann, P. A. Besse, and H. Melchior, "Overlapping-image multimode interference couplers with a reduced number of self-images for uniform and nonuniform power splitting," *Appl. Opt.*, vol. 34, no. 30, pp. 6898–6908, Oct. 1995.

Martin T. Hill (S'96–A'97), photograph and biography not available at the time of publication.

X. J. M. Leijtens, photograph and biography not available at the time of publication.

G. D. Khoe (S'71–M'71–SM'85–F'91), photograph and biography not available at the time of publication.

M. K. Smit (A'93–M'00–SM'01), photograph and biography not available at the time of publication.